JOURNAL OF MODERN OPTICS
2019, VOL. 66, NO. 11, 1206–1214
https://doi.org/10.1080/09500340.2019.1609617

Semi-analytical Monte Carlo simulation for time-resolved light propagating in multilayered turbid media

Ling Xuan Zhu, Xiao Bing Wang, Biao Wang and Yi Wei Hu

Science and Technology on Electromagnetic Scattering Laboratory, Shanghai, People's Republic of China

ABSTRACT

In this study, a Monte Carlo (MC) method for time-resolved light scattering from multilayered turbid media (SMCML) has been developed. This method is particularly suitable for simulating light backscattering from layered media and receiving the time-resolved signal in a finite sensor area, such as ocean detection, photomedicine and photobiology. The classical semi-analytical MC method requires the scattering events to be located in a single-layer medium. To address the multilayer problem, the energy loss mechanism of photons propagating in tissue was analyzed in this study. According to the energy contribution to the detector, only photons that contribute significantly were considered. Simulations were conducted for stochastic turbid media with different optical parameters. Temporal profiles of the echo signal were obtained with a satisfactory convergence. Compared to the classical MC method, the SMCML method can dramatically reduce the computation time by more than two orders of magnitude.

ARTICLE HISTORY
Received 24 December 2018
Accepted 12 April 2019

KEYWORDS
Scattering; Monte Carlo simulation; time resolved; radiative transfer; light propagating

1. Introduction

The Monte Carlo (MC) method is viewed as a classical numerical technique for solving photon propagation in turbid media and has been widely used in many fields such as optical detection, telecommunications, photobiology (*1*,*2*). Whereas, the major drawback of MC is the Inefficient calculation. After years of evolution, a variety of methods for accelerating the MC simulations have been developed, including scaling methods (*3*,*4*), perturbation methods (*5*), and hybrid methods (*6*,*7*). However, there are still some obstacles preventing the realization of this technique to obtain time-resolved signals for a finite detecting area and limited field of view, which is often encountered in the fields of ocean and atmospheric remote detection. Such a low-probability event exponentially increases the time consumption in the MC method, resulting in the difficulty of the simulation converging to a value.

Tinet *et al.* (*8*) adapted the statistical estimator technique to a fast semi-analytical MC model for simulating time-resolved light scattering problems. However, it is only suitable for single-layer tissue because of its designed photon transmission mechanism. Chen *et al.* (*9*,*10*) proposed a controlled MC method in which an attractive point with an adjustable factor increases the efficiency of trajectory generation by forcing photons to propagate along directions more likely to intersect with the detector. However, there is no dedicated formula currently available for calculating the attractive factor, and the statistics could deteriorate in an unfavourable region.

In this paper, we propose a semi-analytical Monte Carlo (SMCML) method to simulate the time-resolved signal in a finite detecting area from light scattering in multilayered turbid media. The classical MC mechanism is applied to generate the moving trajectory and photon energy weight for light propagating in a medium, and an analytical method is used to accumulate the energy contribution. Based on the analysis of photon propagations inside the tissue, different approximations are adapted in the analytical method for the boundary layer and underlayers.

In Section 2, the SMCML is described in detail. Section 3 provides the simulation results using this new method. Our algorithm is verified by applying it to multilayered media of different optical thickness and comparing the computational efficiency to the MCML method. It is found that the SMCML method provides a more stable and reliable shape of the reflected pulse and accelerates the MC simulation.

CONTACT Xiao Bing Wang ht802stesl@outlook.com Science and Technology on Electromagnetic Scattering Laboratory, Shanghai 200090, People's Republic of China

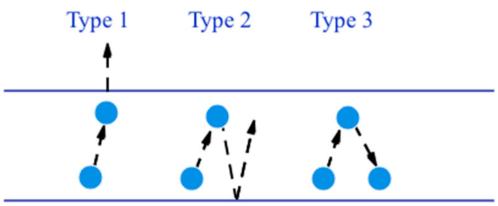

Figure 1. Schematic of three types of photon propagations in medium.

2. Method

For the problem of light propagation in multilayer media, the MC method generates photon transmission trajectory and energy contribution based on random sampling. The probability that a photon will reach the detector comes from all potential arrival paths, However, it is neither realistic nor necessary to considerate countless paths. The traditional MC method simulates various paths through a large number of random samples. Instead, we introduce the analytical method to avoid the computational cost in inefficient path sampling. Further, the principle of the SMCML is to evaluate every possible detected photon and accumulate the major potential contribution.

By analysing the light transport process in the media, we summarize three types of photon propagations, as illustrated in Figure 1. The first propagation type represents the remaining energy that transmits through the layer interface, entering the other layers, or exiting the medium without any reflections. The second type of propagation indicates that the photon is reflected or multi-reflected from the interface of any layer in single-scattering event. The third type of propagation represents the remaining energy in the photon that continually scatters inside the medium layer without any interaction with layer interface. In summary, if a photon exits the medium, the last step must be the propagation of the first and second type.

As illustrated in Figure 2, we divide the medium into two parts, the boundary layer (layer 1), which is nearest to the detector, and the underlayers (layer $2-n$). All three types of propagation situations illustrated in Figure 1 will take place in both the boundary layer and underlayers.

In a MC simulation, the free propagating path length between any two subsequent scattering events is randomly generated with a probability density function $\mu_t \exp(-\mu_t s)$, so the path length is dependent on the extinction coefficient of the medium. In addition, the probability of the energy contribution of the photon is associated with the optical distance between the detector and scattering points (*8*). Based on the above two reasons, most of the detected energy originate from scattering events in the boundary layer, and only some of

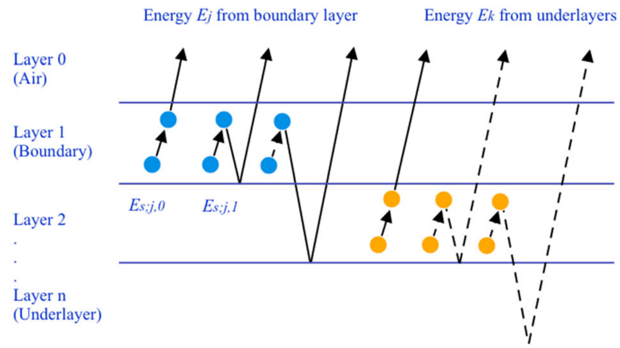

Figure 2. Schematic of three types of photon propagations in medium.

the energy originates from the other layers. Moreover, because of the additional propagation length, photons experiencing multiple reflections or transmissions will lose most of the energy before they are collected. These effects will be further analysed in Section 3.1.

Therefore, the approximation used in this paper consists of two parts. In the first part, for photons whose scattering points originate from the boundary layer, the analytical method consider that these photons experience no more than once reflection before they reach the detector. However the reflection could occur in the boundary layer or in the underlayers. In the second part, for photons whose scattering points originate from the underlayers, analytical method only consider the case that they directly reach the detector without reflection. In Figure 2, the solid line represents the type of propagation we consider and the dashed line represents the ignored contributions.

The classical MC mechanism (*12*) is employed to generate the moving trajectory and light-tissue interactions for each launching photon, including random walking, light absorption and scattering, reflection or transmission at interface. The walking step size and scattering angle will be sampled randomly based on the optical properties of medium and the last scattering event. If it is about to hit an interface, the photon will either transmit through or be reflected from the interface governed by the Snell's law and Fresnel's equations.

The analytical method is calculated before each scattering interaction. As the procedure to simulate the reflection or transmission signal is similar, we demonstrate the SMCML method in light backscattering from multilayered tissue. As shown in Figure 3, light is vertically incident on the multilayered tissue, and a detector is placed at point $M(x_m, y_m, z_m)$ above the medium, with a finite detecting space of round area ΔS and a relevant long media-detector distance.

Based on the analysis above, the total diffused energy E received at the detector is the sum of the E_j contributions

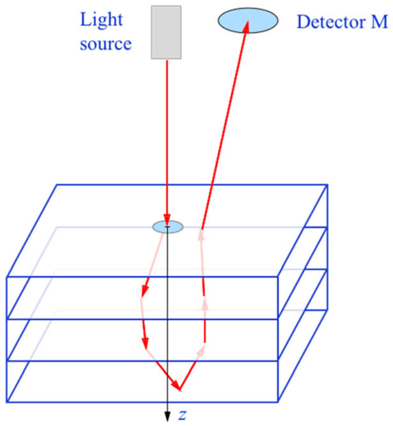

Figure 3. Schematic of photon propagating in multilayered media.

of all the scattering events in the boundary layer and the E_k contributions of all the scattering events in the underlayers:

$$E = \sum_{j=1}^{J} E_j + \sum_{k=1}^{K} E_k, \tag{1}$$

where E_j is the contributions of all the scattering events in the boundary layer, E_k is the contributions of all the scattering events in the underlayers, j represents the jth scattering point in the boundary layer, and k represents the kth scattering point in the underlayers. For these two energy contribution sources, we apply different approximations, which will accelerate the computation and simultaneously guarantee precise results.

2.1. Boundary layer energy collection

In the case of no refractive index matching, the energy contributions of all the scattering points in the boundary layer are from the photons that directly transmit through the medium and the photons that experience only several reflections from the boundary layer.

The energy E_j received without additional scattering events from the scattering point P_j in the boundary layer is

$$E_j = E_{s;j,0} + \sum_{h=1}^{H} E_{s;j,h}, \tag{2}$$

where $E_{s;j,0}$ is the contribution of the first propagation type defined in this paper from scattering point P_j to detector M; $E_{s;j,h}$ is the contribution of the second propagation type, which experiences h reflections at the layer interface. However, each propagation event adds one reflection, greatly decreasing the rate of energy contribution. Therefore, it will be reasonable to consider only one reflection in the propagation event. The simplified calculation of E_j is

$$E_j \approx E_{s;j,0} + E_{s;j,1}, \tag{3}$$

where $E_{s;j,1}$ is the contribution of the second propagation type, which experiences one reflection at the layer interface.

2.1.1. First propagation type in boundary layer

For every scattering point, only a finite solid angle of energy can be collected by the detector. The solid angle depends on the detecting area and distance between the scattering and detector. The angular distribution of scattered energy is characterized by a phase function. Before the photon reaches the detector, the energy is reduced by the extinction in the medium and the reflection at the boundary. The energy $E_{s;j,0}$ from scattering point P_j to detector M is

$$E_{s;j,0} = E_{s;j} f(\vec{\boldsymbol{s}} \cdot \vec{\boldsymbol{m}}, g) \exp(-\mu_t L_j) \frac{\Delta S}{d_j^2} \cdot [1 - R_{1,0}(\alpha_j)], \tag{4}$$

where $E_{s;j}$ is the total energy radiated by the scattering point. The exponential term $\exp(-\mu_t L_j)$ accounts for extinction along the trajectory in the medium, $\mu_t = \mu_a + \mu_s$ is the extinction coefficient, and μ_s and $\mu_a$are the scattering and absorption coefficients, respectively. The parameter ΔS is the detector area and d is the distance between the scattering point and detector. $f(\cos\theta, g)$ is the Henyey–Greenstein phase function (*11*), defined as

$$f(\cos\theta, g) = \frac{1}{4\pi} \cdot \frac{1 - g^2}{2(1 + g^2 - 2g\cos\theta)^{3/2}}, \tag{5}$$

where g is the anisotropy factor ranging from -1 to $+1$ and θ is the scattering angle, defined by $\cos\theta = \vec{\boldsymbol{s}} \cdot \vec{\boldsymbol{m}} \cdot \vec{\boldsymbol{s}}$ is the propagation direction of the incident photon, as shown in Figure 4. $\vec{\boldsymbol{m}}$ is the unit vector defining the direction from the scattering point $P_j(x_j, y_j, z_j)$in the boundary layer to the detector point M:

$$\vec{\boldsymbol{m}} = (u_{mx}, u_{my}, u_{mz}) = \frac{1}{d_j} \cdot (x_m - x_j, y_m - y_j, z_m - z_j), \tag{6}$$

where d_j is the distance between detector position M and the scattering point:

$$d_j = [(x_m - x_j)^2 + (y_m - y_j)^2 + (z_m - z_j)^2]^{1/2}. \tag{7}$$

The Cartesian coordinate system was set up such that the axial dimension, which is perpendicular to the top surface of the baseline medium, corresponds to the z axis,

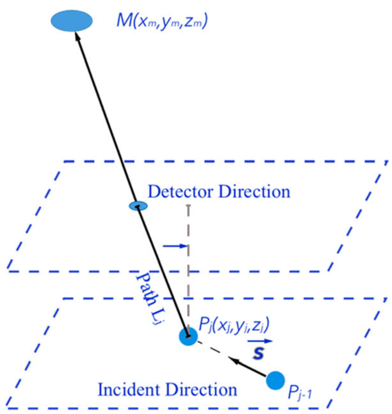

Figure 4. Schematic of scattering angle and step path.

and the x–y plane is parallel to the top surface of the boundary layer.

In the general procedure of MC modelling (*7*), the path length and scattering angle for every step is sampled randomly based on their respective probability distributions. As the detector position $M(x_m, y_m, z_m)$ is located out of the medium, the step path L_j from the scattering point toward the detector only includes the length inside the medium:

$$L_j = \frac{z_j}{u_{mz}}. \tag{8}$$

The angle α_j is defined by $u_{mz} = \cos(\alpha_j)$. The possibility of transmission $[1 - R_{1,0}(\alpha_j)]$ at the boundary between layer 1 and layer 0 is determined by Fresnel's formulas and is an average of the reflectance for the two orthogonal polarization directions (*12*):

$$R(\alpha_i) = \frac{1}{2}\left[\frac{\sin^2(\alpha_i - \alpha_t)}{\sin^2(\alpha_i + \alpha_t)} + \frac{\tan^2(\alpha_i - \alpha_t)}{\tan^2(\alpha_i + \alpha_t)}\right], \tag{9}$$

where α_i is the angle of incidence and α_t is the angle of transmission.

2.1.2. Second propagation type in boundary layer

The energy $E_{s;j,1}$ can be calculated by

$$E_{s;j,1} = \sum_{i=1}^{I} E_{s;j,1,i}, \tag{10}$$

where $E_{s;j,1,i}$ is the contribution of the second propagation type, which experiences one reflection at the ith layer interface. The I parameter is the total layer number of the target medium.

$$E_{s;j,1,i} = E_{s;j} f(\vec{s} \cdot \vec{m}_i, g) \exp(-L_{\text{opt};i}) \frac{\Delta S}{d_{j,i}{}^2} \cdot T_i R_{i,i+1}(\alpha_{j,i}), \tag{11}$$

where the unit vector $\vec{m}_i$, distance $d_{j,s}$ and scattering angle $\alpha_{j,i}$ maintain the same definitions as Equations (6)–(9), but the detector position M changes to the image detector position M_i seen through the ith surface of the lower border, which is $M_i = (x_m, y_m, D_i - z_m)$. $L_{\text{opt};i}$ represents the optical path length inside the layer, which can be calculated by

$$L_{\text{opt};i} = \frac{1}{u_{mz;i}}\left[-\mu_{t,1} z_j + \sum_{i'=1}^{i} 2\mu_{t,i'}(D_{i'} - D_{i'-1})\right], \tag{12}$$

where D_i is the depth of the ith surface of the lower border, $\mu_{t,i}$ is the extinction coefficient of the ith medium layer. T_i represents the total transmission rate in the trajectory, which is

$$T_i = \frac{1}{[1 - R_{0,1}(\alpha_{j,i})]} \prod_{i'=1}^{i} [1 - R_{i,i-1}(\alpha_{j,i})][1 - R_{i-1,i}(\alpha_{j,i})], \tag{13}$$

where $R_{i,i-1}$ is the Fresnel expression for specular reflection for the light hitting the interface between layer i and layer i−1 and accounts for the energy loss in reflection.

2.2. Underlayer energy collection

The calculation of the energy E_k in Equation (1) is similar to the first propagation type in the boundary layer:

$$E_k = E_{s;k} f(\vec{s} \cdot \vec{m}) \exp \times \left(-\sum_{i=1}^{I_s} \mu_{t,i} L_{k,i}\right) \frac{\Delta S}{d_k{}^2} \cdot \prod_{i=1}^{I_s} [1 - R_{i,i-1}(\alpha_k)], \tag{14}$$

where the I_s parameter is the layer number of the scattering point. The subscript i represents the ith layer, $L_{k,i}$ represents the propagation length inside the layer, $\mu_{t,i}$ is the extinction coefficient, and $R_{i,i-1}$ is the specular reflection rate at the interface between layer i and i−1. In addition, the influence of reflections between the underlayers can be added if the optical thickness of the layers is comparable to the free path.

2.3. Time-resolved computation

After each scattering, a photon is allowed to propagate a random distance. The total path length is the sum of every step path length and the final step path from the scattering point toward the detector. Then, the time coordinate for each component of the sum is determined. The relative time-resolved signal $W(\tau)$ can be given as

$$W(\tau) = \frac{1}{N_0}\left[\sum_{j=1}^{J} E_j(\tau, \tau + d\tau) + \sum_{k=1}^{K} E_k(\tau, \tau + d\tau)\right], \tag{15}$$

in which N_0 represents the total number of photons launched and $E(\tau, \tau + d\tau)$ is the weight of each contributed photon with the detected time between τ and $\tau + d\tau$.

3. Simulation results

3.1. Energy contribution

To validate the assumption of analytical method, we test and compare the energy contribution from different positions and different photon propagation types. Each independent simulation was run five times.

3.1.1. Energy contribution in different layers

In this section, different parameters are set to investigate the spatial distribution of the last scattering positions under ideal conditions. Here, we consider a slab model, which is a homogeneous turbid medium restricted by parallel planar interfaces in each layer. Photons are introduced into the slab at the same time to simulate an ultra-short pulse of point light illuminating one of the surfaces perpendicularly. The medium is divided into two layers, but the optical parameters of each layer are the same, including the refractive index between layers. The boundary layer has a thickness of 1 cm and the underlayer has a thickness of 9 cm.

In Table 1, we test the energy contribution to the diffuse reflectance in different layers, the results were given by MCML simulator, created by Wang and Jacques. The parameters are used to described the optical properties in boundary layer. The albedo is denoted by ω_0, and $\omega_0 = \mu_s/\mu_t$. The optical depth (D_{opt}) is $D_{\text{opt}} = \mu_t D$, where D is the layer thickness. P_{boundary} represents the ratio of the energy contribution in the boundary layer (E_{boundary}) to the total diffuse reflectance (R), defined as $P_{\text{boundary}} = E_{\text{boundary}}/R$. These tests were made for a wide range of optical coefficients: the albedo ranging from 0.1–0.9, the optical depth from 0.1–100, the anisotropy factor g from 0.1–0.9.

Comparing the tests in Table 1, Optical thickness plays a major role in each of the influencing factors. As the boundary optical depth increases from 0.1–1, P_{boundary} rises rapidly from 0.28–0.8. When ignoring the effect of layer-to-layer refractive index changes, almost all of the photons that escapes the medium after backscattering originates from regions with optical thickness less than 10. Hence, if the boundary layer optical thickness is greater than 10, sufficient calculation accuracy can be achieved by using only the semi-analytical method described in Section 2.1.

Table 1. Energy contribution in different layers.

Test	D_{opt}	ω_0	g	P_{boundary}
1	0.1	0.9	0.9	0.279
2	0.5	0.9	0.9	0.6
3	1	0.9	0.9	0.8072
4	10	0.9	0.9	1
5	100	0.9	0.9	1
6	1	0.5	0.9	0.8888
7	1	0.1	0.9	0.9095
8	1	0.9	05	0.8121
9	1	0.9	0.1	0.8351

On the contrary, the influence of the asymmetry factor and the albedo is relatively small. The asymmetry factor affects the extent to which the scattering spreads around. When the asymmetry factor increases from 0.1–0.9, P_{boundary} is only reduced by a few percent. The albedo affects the proportion of energy absorbed in each scattering, and as the albedo increases, the energy contribution from deeper position decreases, thereby increasing the ratio of energy contribution from the boundary layer.

3.1.2. Energy contribution from different photon propagation types

In this section, we investigate the contribution of different photon propagation types to the detected energy in scattering. The setting of the light source is the same as in Section 3.1.1. The medium is divided into three layers with thicknesses of 1, 1, and 8 cm, respectively. In Table 2, the optical parameters of each layer are the same except for the refractive index, ω_0 equals to 0.9 and g equals to 0.9. $P_{\text{reflection}}(0)$, $P_{\text{reflection}}(1)$ and P_{count} represent the ratio of the energy contribution from different photon propagation types to the total diffuse reflectance. Where $P_{\text{reflection}}(0)$ stands for the first type propagation, that is, the photon does not experience reflection in the last scattering, and $P_{\text{reflection}}(1)$ stands for the photon propagation that photon only experiences once reflection in the last scattering. P_{count} stands for the photon propagations that SMCML method considerate. The results were given by MCML simulator with 10,000,000 photons launched.

Test 1 to Test 3 compare the relative refractive index changes between the boundary layer and the underlayers. When the optical thickness of the boundary layer is greater than 1, the SMCML method can account for more than 98% of the energy contribution for all three cases. Test 4 to test 7 compare the effects of different optical thicknesses of the boundary layer. It should be pointed out that as the optical thickness of the boundary layer decreases from 1 to 0.1, $P_{\text{reflection}}(1)$ rises from the 0.03–0.93, which means that most photons undergo once

Table 2. Energy contribution from different photon propagation types.

	Optical parameters			Simulation result			
Test	Layer number	n	D_{opt}	$P_{reflection}(0)$	$P_{reflection}(1)$	P_{count}	$P_{boundary}$
1	1	1.1	1	0.9739	0.0261	0.9845	0.705
	2	1.3	1				
	3	1	8				
2	1	1.3	1	0.9487	0.0513	0.9873	0.7709
	2	1.3	1				
	3	1	8				
3	1	1.5	1	0.951	0.0489	0.9845	0.7003
	2	1.3	1				
	3	1	8				
4	1	1.1	0.1	0.0722	0.9264	0.9917	0.9355
	2	1.3	0.1				
	3	1	0.8				
5	1	1.1	0.01	0.0722	0.9264	0.9917	0.9355
	2	1.3	0.01				
	3	1	0.08				
6	1	1.1	10	1	0	1	1
	2	1.3	10				
	3	1	90				
7	1	1.1	100	1	0	1	1
	2	1.3	100				
	3	1	900				

reflection during the scattering process before leaving the medium. But when the boundary layer optical thickness is greater than 10, almost all energy contributions are derived from the first photon propagation type.

3.2. Accuracy of time-resolved detection signal

To test the accuracy of simulating light backscattering from layered media by SMCML algorithm, the time-resolved signal was independently simulated on the three-layered homogeneous turbid medium, in which the same anisotropy factor, refractive indices, layer thickness and light source as used in the Section 3.1.2 test 1 were employed. The optical thickness of the boundary layer ranges from 0.01–100, by changing the extinction coefficient of the medium. The detector is placed 300 cm above the medium, with 5 cm away from the light source in the y-axis direction, and has a round detection area of 20 cm^2. The deviation in the horizontal direction is to avoid receiving specular reflection energy. The intensity of detected signal was normalized as defined in Equation (15).

3.2.1. The intensity of detection signal

In each of MC simulations, 10^8 photons were launched to calculate the relative error (δ) and coefficient of variation (CV). The CV is the ratio of the standard deviation to the mean value. The relative error is defined as

$$\delta = \frac{x - \mu}{\mu}, \tag{16}$$

Where the standard value (μ) is the averaged result from 5 times independent MCML simulations, x is the normalized intensity from SMCML simulation.

Figure 5(a) shows relative error of detection signal normalized intensity from SMCML simulation compared with MCML simulation results. The range of relative error is less than 6% and it comes from the approximation in the analytical formula. The energy contribution of the path without reflection is greater than the true value, and the energy contribution of the path containing the reflection is smaller than the true value.

Figure 5(b) compares the coefficients of variation of the SMCML algorithm and the MCML algorithm. As the optical thickness increases, the simulation results of the MCML algorithm fluctuate and become more and more difficult to converge. On the contrary, the SMCML algorithm can maintain a stable output under various conditions.

3.2.2. Time-resolved signal

In order to demonstrate the confidence of the algorithm, we compare the time-resolved signal of 10^7 and 10^8 photons. The light propagates in the layered medium with the parameters of test 6 in Table 2. The detector collects photons at all angles. Figure 6 shows the simulated time-resolved echo signal, and time starts with the first signal received.

By launching 10^7 photons, the classical MCML simulator still cannot discern a good shape of the reflected pulse at a reasonable quality (Figure 5); only a few photons are collected. In contrast, the SMCML method provides a good evaluation of the pulse with only 10^7 photons.

3.2.3. Spatial distribution of detected energy

The purpose of this part was to analyse how the SMCML algorithm can converge more quickly. Here we record the position and energy of the last scattering of the photon before it was received, and compare the results of the MCML algorithm and the SMCML algorithm. In each MC simulation, 10^8 photons were launched.

Figure 7 shows the logarithm of the energy contribution of the scattering event from any specific depth (z) and horizontal position (x) to the normalized intensity of the detected signal. The upper surface of the medium is located at 0 mm on the z-axis, and the light is incident perpendicularly at 51 cm on the x-axis. The parameter settings for the light source and medium are the same as the test 1 in Table. The spatial resolution is identical in both cases.

It can be seen from the Figure 7 that the calculation results are smoother in spatial distribution in SMCML simulation. Compared to the traditional MC algorithm,

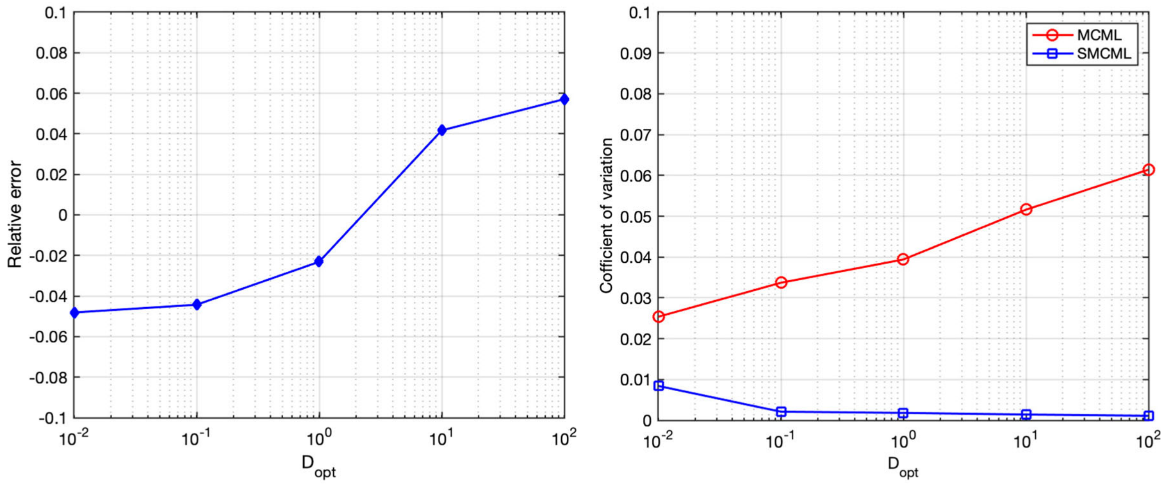

(a) (b)

Figure 5. Relative error (a) and CV (b) as a function of boundary layer optical thickness.

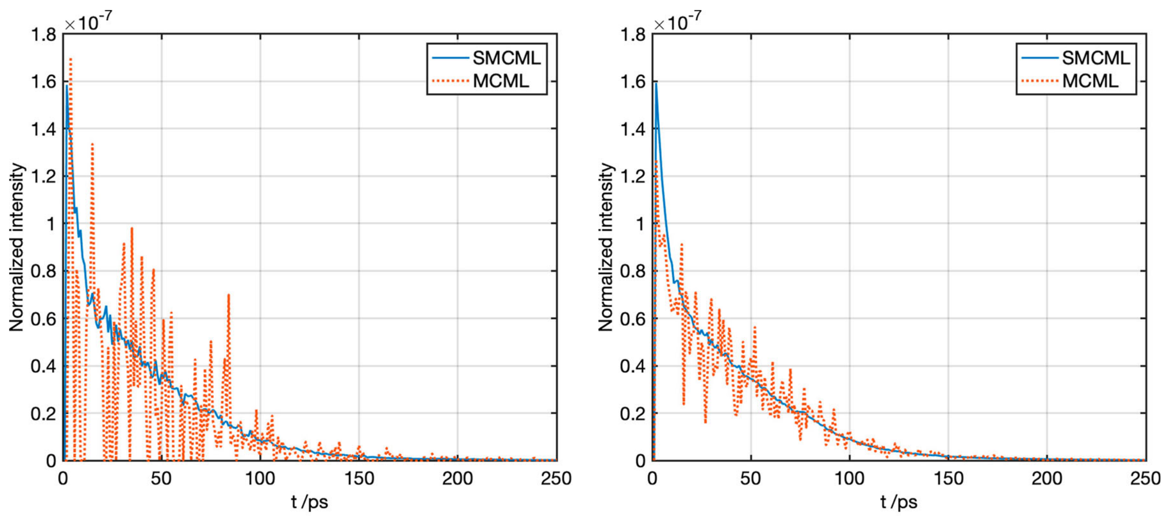

(a) (b)

Figure 6. Time-resolved signal from simulation with (a) 10^7 and (b) 10^8 photons.

the SMCML algorithm can better utilize the subtle information of each scattering event when calculating the detection signal.

4. Computational efficiency

For these comparisons, both MCML and SMCML simulations were performed on the same computer (a 2.9 GHz Intel Core i5 Mac) and used the same compiler (Xcode). For a fair comparison, the same level of programming optimization was used; only the simulation kernels were different.

The major objective of this study is to estimate the efficiency of the SMCML through multilayered turbid media. For an optical path longer than several centimetres, hundreds of scattering events are generally involved, but only a few photons are received at the detector.

In demand of accuracy, the simulation photon number of the classical MC method must be increased, which greatly increases the time consumption. In this study, we compare the accuracy of the MCML and SMCML with different photon numbers and time costs to evaluate the algorithm efficiency. The accuracy R can be defined as

$$R = 1 - \sqrt[2]{\frac{\sum_{i=1}^{m} (y_i - \hat{y}_i)^2}{\sum_{i=1}^{m} (\hat{y}_i)^2}}, \tag{17}$$

where y_i is the test time signal intensity, and we set $\hat{y}_i$ as the simulation result with 10^8 photons, m is the total time

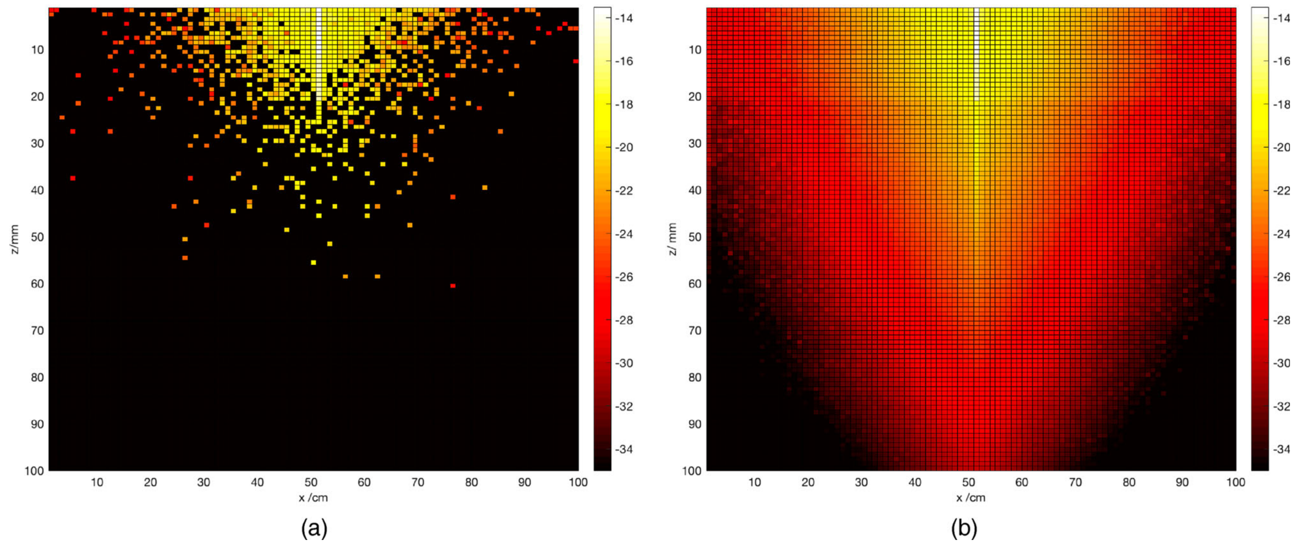

Figure 7. The spatial distribution of the logarithm of the normalized energy contribution to detected energy. (a) MCML simulation result. (b) SMCML simulation result.

bins of time-resolved reflected signal. The time temporal resolution is 1 ps. Here, we compare the accuracy *R* of the time-resolved signal with the parameters settings of test 1, 4 and 6 in Table 2. The optical thickness of boundary layer ranges from 0.1–10. In order to test the algorithm efficiency, we record the launched photon number in each simulation, as shown in Figure 8.

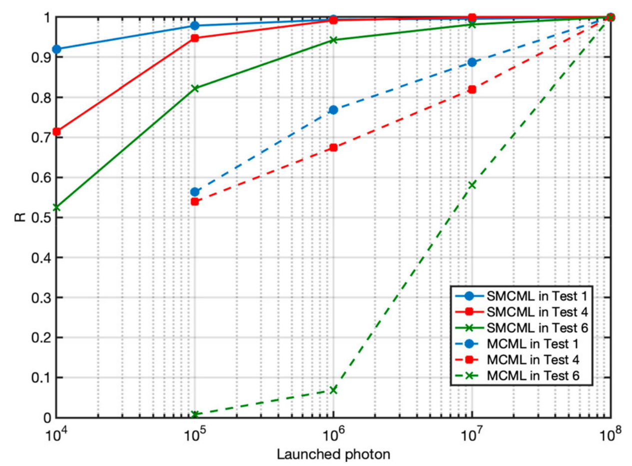

Figure 8. Comparing computation accuracy as a function of launched photon number.

In most cases, the SMCML method requires approximately no more than 10^7 photons to produce a good evaluation of the signal curve compared to 10^8 or even more photons in the MCML. The SMCML algorithm is especially suitable for processing photon radiation transmission in strong scattering media. Because in strong scattering media, simulation takes longer time to converge time-resolved reflected signal. When the optical thickness of a single layer is greater than 10 (like test 6), it takes hours to finish a 10^8 photons simulation in the MCML, while the received signal is still fluctuating. However, by adopting the SMCML method, the number of photons required can be saved by a hundred times, and the simulation time can be saved by tens of times in different scenarios.

5. Conclusion

The SMCML method presented in this paper is more stable and reliable than classical MC simulations for the hard convergence problem in multilayered turbid media. In classical MC methods, we have seen photons that are traced but do not intersect the detector. The general approach of the SMCML is that it considers a method to analytically evaluate the energy distribution in every scattering event so that more photons reach the detector, thus increasing the number of launched photons and thereby reducing the statistical error in the estimated quantity while simultaneously reducing the number of wasted photons. This will improve applications such as oceanic and atmospheric optical detection and may even lead to new applications that are not efficient using current technology.

Compared with other hybrid methods (*13–15*), the SMCML algorithm solves the problem of photons repeatedly crossing the internal interface of multilayer media by MC sampling photon trajectories. It does not need to distinguish between high scattering regions and low scattering regions. On the other hand, compared with the method proposed by Tinet *et al.* (*8*), the SMCML algorithm does not require the post-processing calculations to be performed after all photons have been computed and stored. The SMCML algorithm is suitable for processing the problem of light transmission in a medium with a boundary optical thickness of 0.01 or more. In this case, the detected simulated echo signal can converge quickly, especially advisable for simulating high-scattering medium.

As the former MC process is separated by the analytical mechanism in the SMCML, the algorithm could be grafted with many forms of MC simulators. To simulate fluorescence emission, one additional parameter, the fluorescence quantum yield, could be added to the SMCML. To simulate bioluminescence, the external light source could be changed to a distribution of bioluminescent sources.

However, the SMCML method might cause errors if the elements of the media surface change significantly in a small area. To overcome this limitation, the analytical method of photon contribution for tissue models including the heterogeneities of complex tissue structures require further investigation.

To conclude, we have proposed a novel MC method based on the semi-analytical evaluation of the photon energy distribution. The method is verified by comparing to conventional single-layer and multilayer media. For barely detected time-resolved signals, its advantages are manifested by providing meaningful simulation results.

Disclosure statement

No potential conflict of interest was reported by the authors.

ORCID

Xiao Bing Wang http://orcid.org/0000-0001-9332-2428

References

(1) Vaudelle, F.; L'Huillier, J.-P.; Askoura, M.L. Light Source Distribution and Scattering Phase Function Influence Light Transport in Diffuse Multi-Layered Media. *Opt. Commun.* 2017, *392*, 268–281.
(2) Zhu, C.; Liu, Q. Review of Monte Carlo Modeling of Light Transport in Tissues. *J. Biomed. Opt.* 2013, *18*, 50902.
(3) Graaff, R.; Koelink, M.H.; de Mul, F.F.M.; Zijistra, W.G.; Dassel, A.C.M.; Aarnoudse, J.G. Condensed Monte Carlo Simulations for the Description of Light Transport. *Appl. Opt.* 1993, *32*, 426–434.
(4) Kienle, A.; Patterson, M.S. Determination of the Optical Properties of Turbid Media from a Single Monte Carlo Simulation. *Phys. Med. Biol.* 1996, *41*, 2221–2227.
(5) Seo, I.; You, J.S.; Hayakawa, C.K.; Venugopalan, V. Perturbation and Differential Monte Carlo Methods for Measurement of Optical Properties in a Layered Epithelial Tissue Model. *J. Biomed. Opt.* 2007, *12*, 014030.
(6) Flock, S.T.; Wilson, B.C.; Patterson, M.S. Hybrid Monte Carlo – Diffusion Theory Modelling of Light Distributions in Tissue, Proc. SPIE 0908, 20–28, 1988.
(7) Wang, L.; Jacques, S.L. Hybrid Model of Monte Carlo Simulation and Diffusion Theory for Light Reflectance by Turbid Media. *J. Opt. Soc. Am. A Opt. Image Sci.* 1993, *10*, 1746–1752.
(8) Tinet, E.; Avrillier, S.; Tualle, J.M. Fast Semianalytical Monte Carlo Simulation for Time-Resolved Light Propagation in Turbid Media. *J. Opt. Soc. Am. A Opt. Image Sci.* 1996, *13*, 1903–1915.
(9) Chen, N.G.; Bai, J. Estimation of Quasi-Straightforward Propagating Light in Tissues. *Phys. Med. Biol.* 1999, *44*, 1669–1676.
(10) Chen, N. Controlled Monte Carlo Method for Light Propagation in Tissue of Semi-Infinite Geometry. *Appl. Opt.* 2007, *46*, 1597–1603.
(11) Kamiuto, K. Study of the Henyey-Greenstein Approximation to Scattering Phase Functions. *J. Quant. Spectrosc. Radiat. Transf.* 1987, *37*, 411–413.
(12) S. L. Jacques and L. Wang, *Monte Carlo Modeling of Light Transport in Tissues* (Springer US, 1995), pp. 131–146.
(13) Wang, L.H.V. Rapid Modeling of Diffuse Reflectance of Light in Turbid Slabs. *J. Opt. Soc. Am. A Opt. Image Sci.* 1998, *15* (4), 936–944.
(14) Hayashi, T.; Kashio, Y.; Okada, E. Hybrid Monte Carlo-diffusion Method for Light Propagation in Tissue with a Low-scattering Region. *Appl. Opt.*. 2003, *42* (16), 2888–2896.
(15) Donner, C.; Jensen, H.W. Rapid Simulation of Steady-State Spatially Resolved Reflectance and Transmittance Profiles of Multilayered Turbid Materials. *J. Opt. Soc. Am. A Opt. Image Sci.* 2006, *23* (6), 1382–1390.